



On the definition of geometric imperfections in the F.E. modelling of local buckling in hot-rolled channel sections

Morane C. M. Wack¹, Oudom Chhoeng², Robert Tremblay³, Nicolas Boissonnade⁴

Abstract

The present paper investigates the influence of geometric imperfections on the local buckling response of hot-rolled steel channel sections under compression. There are very little recommendations and guidelines on the design requirements of local geometric imperfections in the context of finite elements modeling. As cross-sectional behavior can have a significant influence on the compressive strength of a member, it is of great importance to assign the right shape and amplitude of local geometric imperfections. Accordingly, this paper aims to provide a consistent and reliable method to numerically model local geometric imperfections in hot-rolled steel channel sections subjected to axial compression. Shell finite element models including geometric imperfections, residual stresses, and fillet radius in cross-sections corners, were developed and validated against stub column test with parallel flanges channel sections. Based on the validated finite element models, numerical parametric studies were performed to assess the effects of various imperfections' shapes, periods and amplitudes on several cross-sections with different width-to-thickness ratios. Safe and reliable recommendations were then provided to better account for local geometric imperfections in finite elements modeling of channel sections under compression.

1. Introduction

The manufacturing processes and transportation conditions of steel members can introduce initial imperfections, causing deviations from their expected ideal shape. These imperfections' nature and their influence depend on the member geometry (open or closed sections, double or mono-symmetric) and the loading conditions. Consequently, they can lead to premature yielding or buckling, reducing the ultimate capacity of hot-rolled steel members under compression and leading to a precipitate failure. The exact shape and amplitude of initial imperfections are generally unknown and assuming the worst-case scenario by combining the most unfavorable shape with fabrication tolerances can be overly conservative and result in expensive constructional costs.

¹ PhD Candidate, Polytechnique Montreal, <morane-chloe.mefande-wack@polymtl.ca>

² PhD Candidate, Polytechnique Montreal, <oudom.chhoeng@polymtl.ca>

³ Professor, Polytechnique Montreal, <robert.tremblay@polymtl.ca>

⁴ Professor, Laval University, <nicolas.boissonnade@gci.ulaval.ca>

With advanced finite element software, implementing geometric imperfections in finite element models has become a significant challenge. A common method (Dawson and Walker 1972) is to assume the shape of geometric imperfections distribution as equivalent to the lowest buckling mode obtained from a linear buckling analysis. This mode is then scaled with an amplification factor that is either the maximum value measured experimentally or an equivalent value used in parametric studies. A general expression of the amplitude of the local imperfections, ω_0 , as derived in Eq. 1, is based on Dawson and Walker's (Dawson and Walker 1972) previous formulation. This expression involves the thickness of the plate, t , the material's 0.2% proof stress, $\sigma_{0.2}$, and the plate's critical buckling stress σ_{cr} .

$$\omega_0/t = \gamma(\sigma_{0.2}/\sigma_{cr}) \quad (1)$$

Dawson and Walker (Dawson and Walker 1972) conducted linear regression analyses to determine the most suitable value for the amplitude, finding a best fit with $\gamma = 0.2$, corresponding to a coefficient of determination $R^2 = 0.025$. Later, Gardner (Gardner 2004) achieved a better fit with $\gamma = 0.023$ and a closer-to-unity $R^2 = 0.22$, thus providing a more accurate prediction. Schafer and Peköz (Schafer and Peköz 1998) studied geometric imperfections in cold-formed steel members and proposed expressions for local geometric imperfections' amplitudes using simple rules of thumb applied to width-to-thickness ratios (w/t) less than 200 and thickness less than 3mm. However, after acknowledging that these conditions do not always represent the full range of possibilities, they also conducted a probabilistic study that treated the maximum imperfection magnitude as a random variable. To analyze the periodicity in the measured imperfections, they generated an imperfection spectrum using the Fourier transform. While this generalized imperfection pattern was consistent with the experimental observations, this approach is impractical for design due to the large number of analyses required.

Greiner (Greiner et al. 2009) suggested a predictive shape for initial local geometric imperfections by modifying the nodal coordinates to follow a sine shape. This method was later adopted by Nseir (Nseir et al. 2016) for hollow sections, and Gerard (Gerard et al. 2019) for I-sections. They investigated the influence of sine shapes' periods and amplitudes on local imperfections and compared the cross-sectional resistances obtained to those with models considering eigenmode shapes as initial imperfection shapes. The period and amplitudes depended on the web and flanges thickness that are respectively, $a_w = h - 2t_f - 2r$ and $a_f = b - t_w - 2r$ for an I-section, where h is the height of the profile, b the width of the profile, t_f the thickness of the flange, t_w the thickness of the web and r the fillet radius (Gerard et al. 2019).

Design codes provide different recommendations for the numerical modeling of local geometric imperfections. The American Specification for Structural Steel Building, AISC 360 (2022), recommends using the permissible construction tolerances outlined in the Code of Standard Practice, AISC 303 (2022), as the amplitude of geometric imperfections. However, it does not provide guidance on the shapes of these imperfections or the appropriate method for incorporating them into finite element analyses. The Canadian standard for the Design and construction of steel structures, CSA S16 (2024), suggests modeling local geometric imperfections as a sine or a cosine function, depending on the boundary conditions, with amplitudes equal to the permissible

tolerances specified in CSA G40.20/G40.21 (R2023) or the applicable ASTM standard, A6/A6M (R2023). The European standards for plated structural elements, EN 1993-1-5 (2006), suggests using the shape of the lowest eigenmode with an amplitude equal to the minimum value between $a/200$ and $b/200$ (a and b refer to the height and width of the plate, as shown in Fig. 1) or 80% of geometric fabrication tolerances. EN 1993-1-5 also addresses the combination of initial imperfections, including geometric imperfections and residual stresses. Among the imperfections, one is selected as the leading imperfection with its full amplitude, while the other accompanying imperfections' amplitudes are reduced by 30%. However, the identification of the leading imperfection is not further discussed.

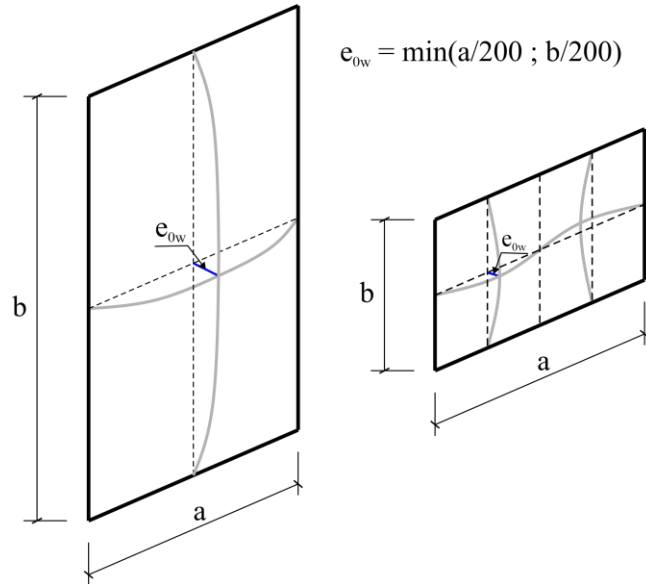


Figure 1: Equivalent local geometric imperfections according to EN 1993-1-5 (2006)

This paper investigates the influence of local geometric imperfections on hot-rolled channel sections, examining the shape and amplitude of initial imperfections to provide recommendations for finite element modeling. Section 2 describes the numerical modeling process of non-linear finite element models and presents a comparison of experimental test results with numerical results assuming different imperfection shapes. Section 3 discusses the influence of various imperfection shapes and amplitudes on the compressive resistance of several slender cross-sections. Section 4 provides recommendations for the definition of local geometric imperfections in finite element models.

2. Numerical modelling

2.1. Development of finite element models

Suitable finite element models have been developed through the software package ABAQUS 2023 and later validated against experimental results. Linear buckling analyses (LBA) and geometric and material nonlinear with imperfection analyses (GMNIA) with displacement control, were carried out to model the behavior of channel sections. The quadrilateral shell element with reduced integration, S4R, was selected to model the finite element models as it has been shown in the literature to be suitable for similar studies (Nseir 2016, Yun 2016, Gérard 2019). After performing mesh sensitivity studies, a mesh size corresponding to $1/10^{\text{th}}$ of the flange width with an aspect ratio of 1 (width/length = 1), exhibited sufficient accuracy while maintaining computational

efficiency and was therefore adopted for all models. To account for the non-negligible extra torsional stiffness due to the fillet radius area in hot-rolled sections and subtract the overlapping area as shown in Fig. 2 (Li et al. 2022), additional hollow beam sections were added at the centroid level of the fillet radius area and implemented with the three-dimensional beam element, B31. Moreover, the fillet radius in hot-rolled sections helps to prevent local buckling within the web-to-flange transition zones. Consequently, extra stiff spring elements were introduced into the model as depicted in Fig. 2 (Li et al. 2022).

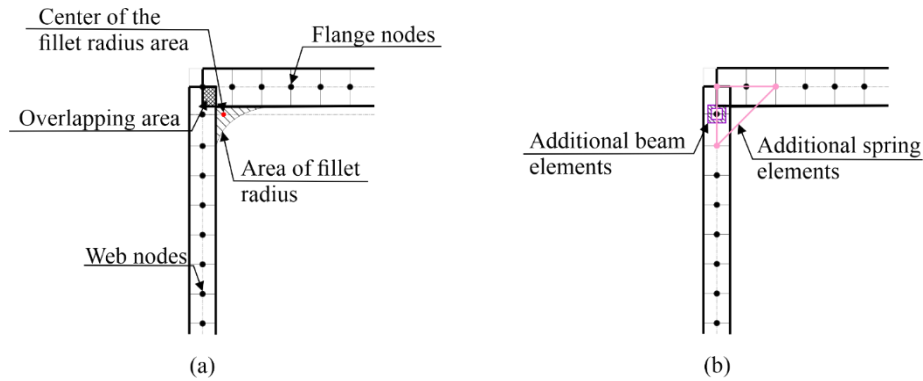


Figure 2: Fillet radius area of hot-rolled sections – (a) real geometry – (b) modeled geometry

Experimental boundary conditions were used for model validation, while fork-type support conditions were considered for the parametric studies (see Fig. 3). Reference points (RPs) were defined at the geometric centroids of both end cross-sections, and rigid body constraints were created between the RPs and the end sections, allowing all degrees of freedom of the end nodes of the model to be governed by the RPs. The boundary and loading conditions were assigned to the RPs to ensure an even application to the end sections. Torsional rotations and out-of-plane displacements about both principal axes at the members' end section (i.e., $u_x = u_y = \theta_z = 0$) were prevented at both end sections. Additionally, axial translation was set free on the loaded end and prevented on the other end, as illustrated in Fig. 3. A non-zero longitudinal distance between the reference point and the end-sections was considered to replicate experimental support conditions, while this distance was set to zero during parametric studies.

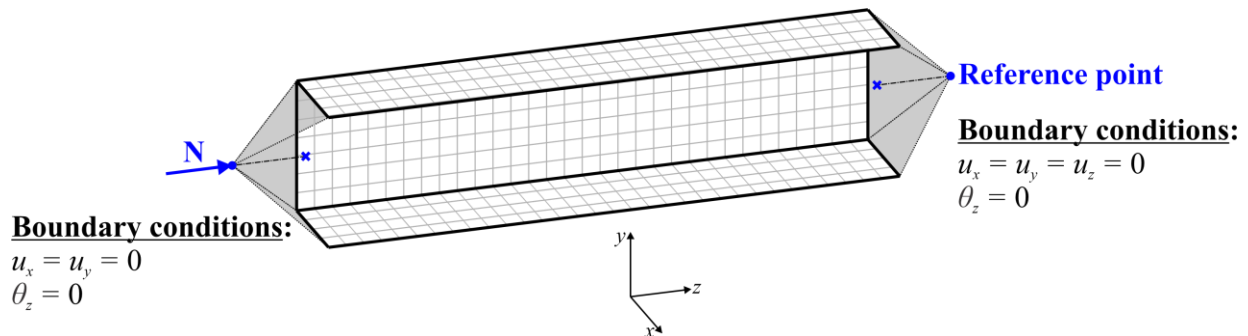


Figure 3: Fork-type support conditions used in parametric studies

The quad-linear material model suggested by Yun (Yun 2017) was adopted in this study. The nominal values of stresses, σ_{nom} , and strains, ε_{nom} , were converted into true stresses, σ_{true} , and plastic strains, ε_p , according to Eq. 2.

$$\begin{aligned}\sigma_{true} &= \sigma_{nom} (1 + \varepsilon_{nom}) \\ \varepsilon_p &= \ln(1 + \varepsilon_{nom}) - \sigma_{true} / E\end{aligned}\quad (2)$$

No reliable residual stress measurements on hot-rolled channel sections are known by the author to this date. The residual stress pattern considered in the present paper was mathematically derived by Beyer (Beyer 2017), based on a pattern that was already proposed and used in many previous studies (Lindner and Glitsch 2004, Snijder et al. 2008) to ensure that all the equilibrium equations are verified.

To account for local geometric imperfections, two approaches are discussed in this paper:

- (i) Approach 1: introducing imperfections through the modification of nodal coordinates to follow a sine shape in both directions of the cross-section's plates for different sets of halfwave lengths and amplitudes as defined by Table 1.
- (ii) Approach 2: introducing imperfections through the first eigenmode shape obtained from a linear buckling analysis, with varying amplitudes.

Table 1 Characteristics of the various sets of local geometric imperfections considered in this study

n°	Case	Halfwave length	Amplitude web	Amplitude flange	Half-wave number
1	$HWL = a_{avg} / L = 5a_{avg} / Amp. = a_{pp} / 200$	a_{avg}	$a_w / 200$	$a_f / 200$	5
2	$HWL = a_{avg} / L = 3a_{avg} / Amp. = a_{pp} / 200$	a_{avg}	$a_w / 200$	$a_f / 200$	3
3	$HWL = a_{avg} / L = 2a_{avg} / Amp. = a_{pp} / 200$	a_{avg}	$a_w / 200$	$a_f / 200$	2
4	$HWL = a_f / L = 3a_f / Amp. = a_{pp} / 200$	a_f	$a_w / 200$	$a_f / 200$	3
5	$HWL = a_w / L = 3a_w / Amp. = a_{pp} / 200$	a_w	$a_w / 200$	$a_f / 200$	3
6	$HWL = a_{pp} / L = 3a_{avg} / Amp. = a_{pp} / 200$	a_{pp}	$a_w / 200$	$a_f / 200$	Variable
7	$HWL = a_{avg} / L = 3a_{avg} / Amp. = a_{pp} / 100$	a_{avg}	$a_w / 100$	$a_f / 100$	3
8	$HWL = a_{avg} / L = 3a_{avg} / Amp. = a_{pp} / 400$	a_{avg}	$a_w / 400$	$a_f / 400$	3
9	$HWL = a_{avg} / L = 3a_{avg} / Amp. = a_{avg} / 200$	a_{avg}	$a_{avg} / 200$	$a_{avg} / 200$	3
10	$HWL = a_{avg} / L = 3a_{avg} / Amp. = a_f / 200$	a_{avg}	$a_f / 200$	$a_f / 200$	3
11	$HWL = a_{avg} / L = 3a_{avg} / Amp. = a_w / 200$	a_{avg}	$a_w / 200$	$a_w / 200$	3

In both cases, the full amplitudes of geometric imperfections were considered and the reduction of 30% prescribed by EN 1993-1-5 was disregarded although residual stresses were considered. Fig. 4 illustrates the different sets of imperfections considered in the first approach. In this case, halfwave lengths and amplitudes are defined by the buckling length of the cross-sections' plates. For hot-rolled channel sections, buckling lengths of flanges and web are respectively

$a_f = 2 \times (b - t_w - r)$ and $a_w = h - 2t_f - 2r$, where b refers to the width of the profile, h to the height of the profile, t_w to the thickness of the web, t_f to the thickness of the flange and r to the fillet radius. Therefore, a case denoted as “ $HWL = a_{pp} / L = 3a_{avg} / Amp. = a_{pp} / 200$ ” refers to a member with an initial local imperfection pattern comprising 3 half-waves, each with a length equal to the corresponding plate’s characteristic buckling length and an amplitude equal to $1/200^{\text{th}}$ of the average between the web buckling length, a_w and the flanges buckling lengths, a_f defined by Eq. 3.

$$a_{avg} = (a_f + a_w) / 2 \quad (3)$$

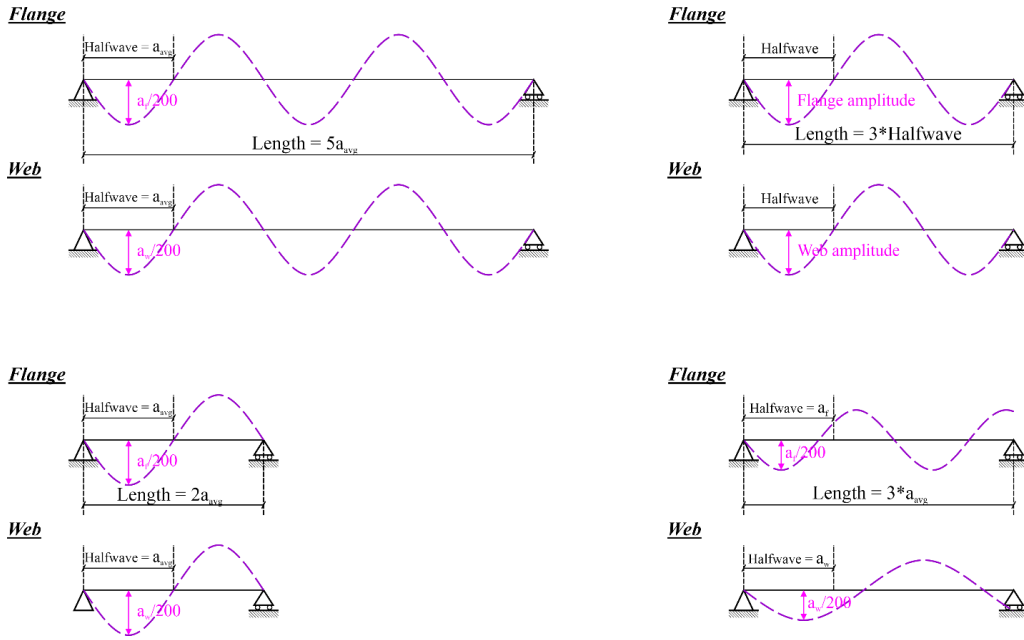


Figure 4: Sine-shape imperfections of cases 1) specified in Table 1 on the upper left; cases 2), 4), 5), 7), 8), 9), 10) and 11) on the upper right; case 3) on the lower left; case 6) on the lower right

2.2. Comparison of numerical models with experimental data

Through an extensive literature review, 26 stub column test data (Li 2023) were gathered to compare different initial geometric imperfection shapes with the measured imperfections during the experimental tests. These tests consisted of hot-rolled channel sections including C80x40x5, C100x50x5 and C100x50x6, from grade EN 1.4301 austenitic stainless-steel sheets subjected to simple and combined loads. Table 2 reports the key parameters and results of these tests, and a typical test setup is illustrated by Fig. 5.

Among the cases described in Table 1, only cases 2, 4, 5, and 6 are considered in this comparative study to assess the effect of the sine shapes periods. Two additional cases, based on the second approach, are also included in the study with the local geometric imperfections amplitude equal to the $1/200^{\text{th}}$ of the average buckling, $Amp. = a_{avg} / 200$, and the measured amplitudes, w_0 . Figs. 6 and 7 show examples of the different initial geometric imperfection shapes considered for

specimen C1-S1, introduced through sine shape functions and first eigenmode shapes, respectively.

Table 2: Test data and corresponding sine shapes periods and amplitudes.

Specimen ID	Load type	b	h	t	r	h/b	w_0	a_f	a_w	a_{avg}	$a_f/200$	$a_w/200$
		(mm)	(mm)	(mm)	(mm)	(-)	(mm)	(mm)	(mm)	(mm)	(mm)	(mm)
C1-S1	N	39.75	80.46	4.79	4.74	2.02	0.03	60.44	61.40	60.92	0.30	0.31
C1-S2	N	39.8	80.39	4.72	4.75	2.02	0.05	60.66	61.45	61.06	0.30	0.31
C2-S1	N	49.75	98.91	4.8	4.84	1.99	0.04	80.22	79.63	79.93	0.40	0.40
C2-S2	N	49.69	98.93	4.72	4.76	1.99	0.04	80.42	79.97	80.20	0.40	0.40
C3-S1	N	49.15	100.11	5.62	5.61	2.04	0.06	75.84	77.65	76.75	0.38	0.39
C3-S2	N	49.18	100.16	5.72	5.74	2.04	0.05	75.44	77.24	76.34	0.38	0.39
C1	N + M _y	49.65	98.93	4.82	4.91	1.99	0.03	79.84	79.47	79.66	0.40	0.40
C2	N + M _y	49.62	98.99	4.79	4.85	1.99	0.04	79.96	79.71	79.84	0.40	0.40
C3	N + M _y	49.62	98.99	4.79	4.87	1.99	0.04	79.92	79.67	79.80	0.40	0.40
C4	N + M _y	49.75	98.95	4.77	4.9	1.99	0.04	80.16	79.61	79.89	0.40	0.40
C5	N + M _y	49.61	98.97	4.73	4.63	1.99	0.04	80.5	80.25	80.38	0.40	0.40
RC1	N + M _y	49.74	99.05	4.86	4.77	1.99	0.03	80.22	79.79	80.01	0.40	0.40
RC2	N + M _y	50.27	99.01	4.79	4.94	1.97	0.04	81.08	79.55	80.32	0.41	0.40
RC3	N + M _y	49.59	98.97	4.75	4.85	2.00	0.03	79.98	79.77	79.88	0.40	0.40
RC4	N + M _y	49.79	98.91	4.71	4.66	1.99	0.04	80.84	80.17	80.51	0.40	0.40
RC5	N + M _y	49.65	98.91	4.76	4.64	1.99	0.03	80.5	80.11	80.31	0.40	0.40
A1	N + M _x	40.52	80.56	5.06	4.95	1.99	0.05	61.02	60.54	60.78	0.31	0.30
A2	N + M _x	40.13	80.79	5.07	4.88	2.01	0.04	60.36	60.89	60.63	0.30	0.30
A3	N + M _x	40.45	80.6	5.01	4.96	1.99	0.03	60.96	60.66	60.81	0.30	0.30
A4	N + M _x	40.14	80.47	4.93	4.91	2.00	0.04	60.6	60.79	60.70	0.30	0.30
A5	N + M _x	39.97	80.41	4.83	4.82	2.01	0.05	60.64	61.11	60.88	0.30	0.31
B1	N + M _x	49.54	98.75	4.85	4.87	1.99	0.03	79.64	79.31	79.48	0.40	0.40
B2	N + M _x	49.76	98.98	5.02	4.95	1.99	0.04	79.58	79.04	79.31	0.40	0.40
B3	N + M _x	49.77	98.98	5.07	5.01	1.99	0.05	79.38	78.82	79.10	0.40	0.39
B4	N + M _x	49.63	98.99	5.07	4.98	1.99	0.03	79.16	78.89	79.03	0.40	0.39
B5	N + M _x	49.6	98.92	4.99	4.89	1.99	0.03	79.44	79.16	79.30	0.40	0.40

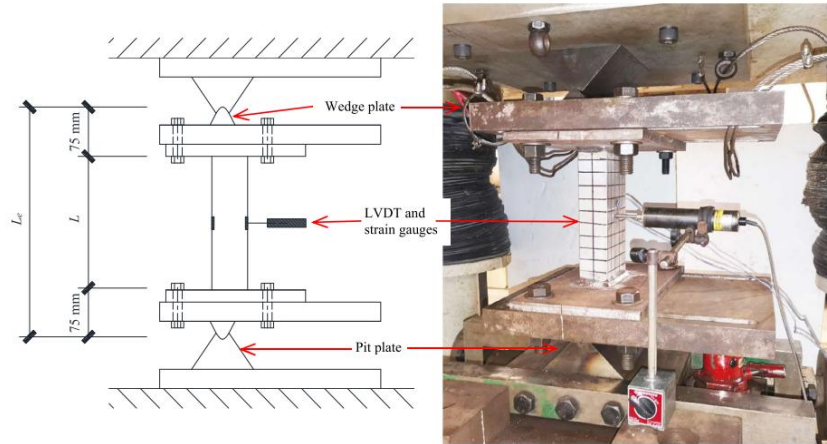


Figure 5: Typical experimental testing setup for specimens under combined loads (Li 2023)

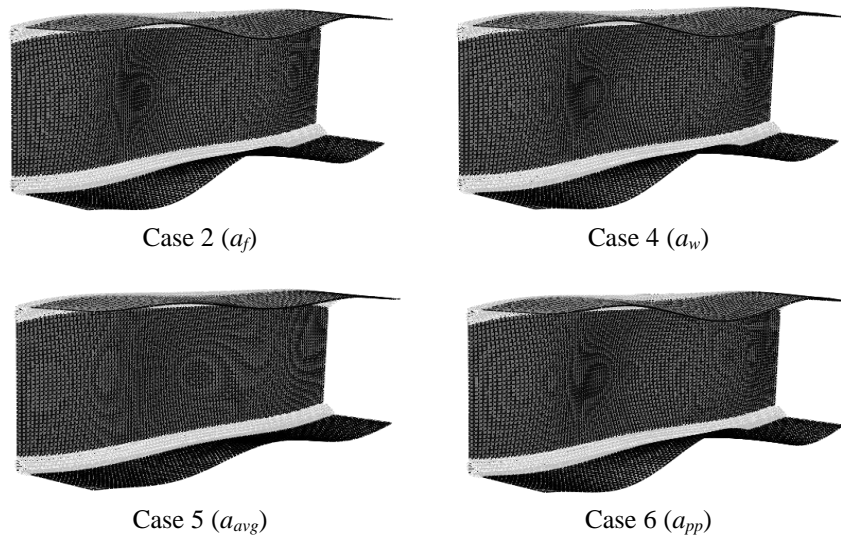


Figure 6: Initial imperfections introduced through sine shapes for specimen C1-S1

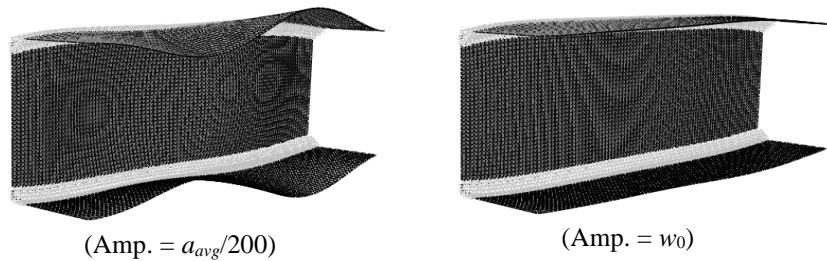


Figure 7: Initial imperfections introduced through eigenmode shapes for specimen C1-S1

Figs. 8 to 10 present a comparison between experimental cross-sectional resistances and their numerical counterparts. The ratios of the ultimate load obtained from FE analyses, P_{FEA} , to the experimental load, P_{EXP} , highlight the divergences between numerical and experimental

resistances due to the imperfection pattern considered. It indicates the accuracy and safety levels of the models as well as the reliability and consistency of the sets of imperfections.

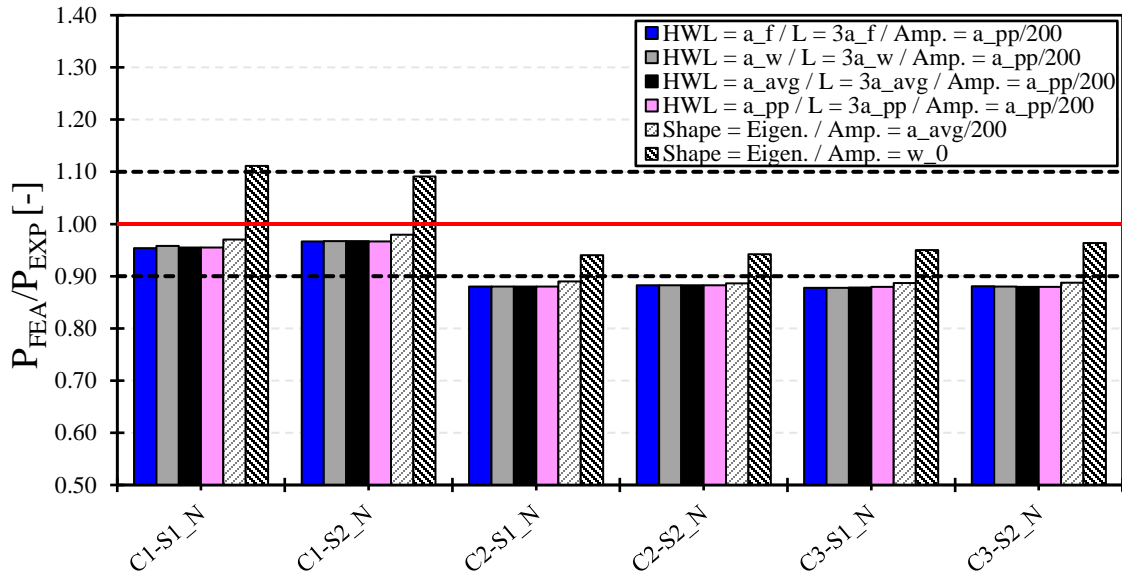


Figure 8: Ultimate capacity of channel sections under pure compression with different imperfection shapes

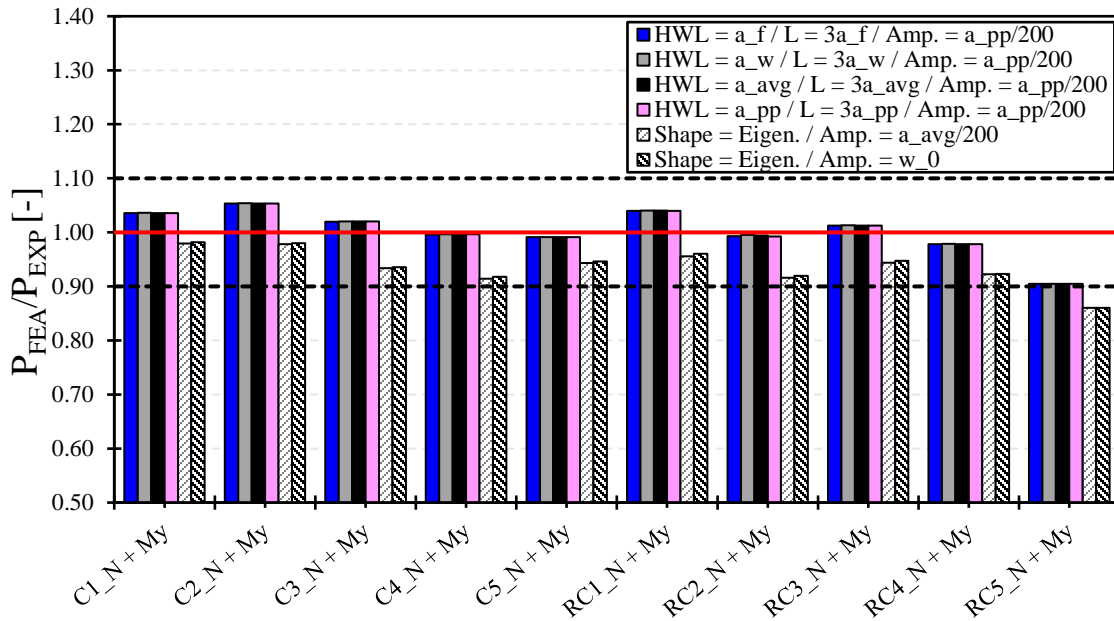


Figure 9: Ultimate capacity of channel sections under minor-axis combined loading with different imperfection shapes

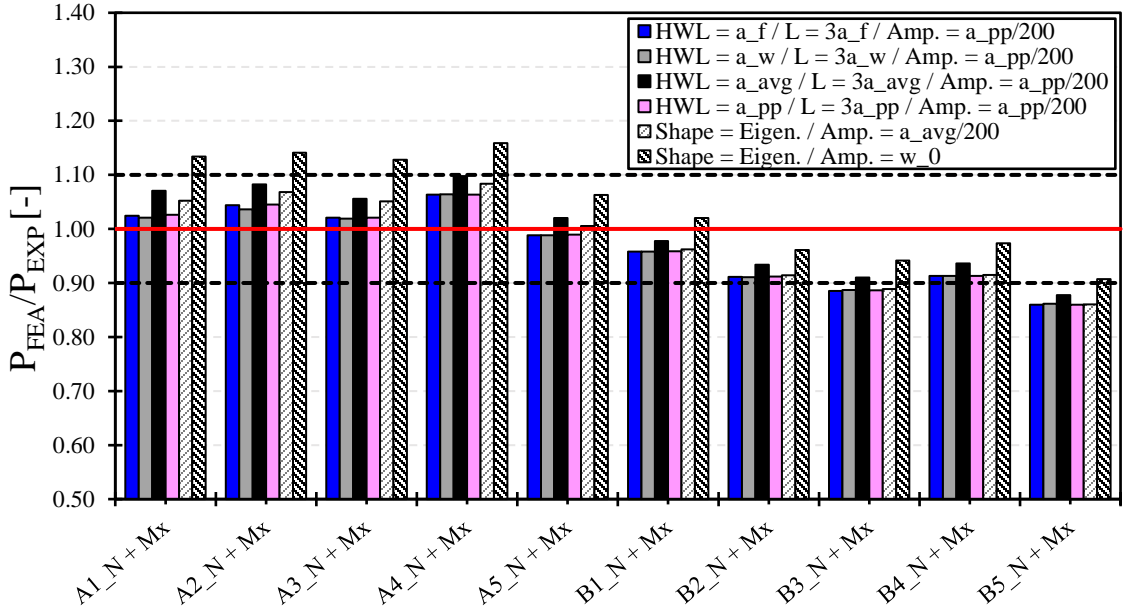


Figure 10: Ultimate capacity of channel sections under major-axis combined loading with different imperfection shapes

These figures lead to the following conclusions:

- (i). When sine shapes are used to model geometric imperfections, the period of the sine shape appears to have a negligible influence on the cross-sectional capacity in case of pure compression (See Fig. 8) and minor-axis combined loading (See Fig. 9). While the chosen amplitude, $a_{pp}/200$ leads to accurate results with the combined load cases, especially the minor-axis combined loading, it leads to over-conservative results in case of pure compression.
- (ii). When the first eigenmode shape is used with an amplitude of $a_{avg}/200$, the ultimate capacities are very close to the ultimate capacities obtained with the sine shapes for members under pure compression (See Fig. 8) and major axis combined loadings (See Fig. 10). With both approaches, the amplitudes are quite similar according to Table 2. Hence, this highlights the fact that the shape of the local geometric imperfections might not be a significant parameter compared to the amplitude considered. For both loading cases, when the measured amplitudes, w_0 , are combined with the first eigenmode shapes, the ultimate capacities are higher than any other case – as expected – because the values of w_0 are lower than the amplitudes defined by the buckling length (See Table 2).
- (iii). While the second approach showed greater consistency in the case of pure compression and major axis combined loading, it appears much less reliable in the case of minor axis combined loading, regardless of the amplitude under consideration as shown in Fig. 9.

Overall, most results of the ratios P_{FEA}/P_{EXP} are in a satisfactory range and the lowest values can be result either from (i) the divergence in lengths between tests and FE analyses or (ii) the residual

stress and geometric imperfections patterns considered in the FE models. Nevertheless, this study is of great relevance regarding the topic of the current paper as it highlights the reliability of several sets of imperfections. A deeper study on the influence of the period and amplitude of each set of imperfections; with different width-to-height and width-to-thickness ratios, is performed in the following section.

3. Parametric studies

A comprehensive study delved into axially loaded hot-rolled channel sections, examining various dimensions and plate slenderness. The numerical models used linear constraints previously introduced in this paper and included sections with different width-to-thickness ratios. The geometry of the ten cross-sections investigated are summarized in Table 3. Three of these cross-sections are sourced from the AISC15 catalog, while the remaining seven are specifically designed to achieve high cross-sectional slenderness according to AISC 360, CSA S16, and Eurocode 3 Part 1-1. Two steel grades were considered for each cross-section: CSA G40.21 260W ($F_y = 260MPa$) and CSA G40.21 400W ($F_y = 400MPa$).

Table 3 Geometry of the studied hot-rolled channel sections

Number	Designation	Source	b (mm)	h (mm)	t_f (mm)	t_w (mm)	r (mm)	a_w (mm)	a_f (mm)	h/b (-)
1	MC10X8.4	AISC15	38.10	254.00	7.11	4.32	11.38	217.02	39.22	6.67
2	MC12X10.6	AISC15	38.10	304.80	7.85	4.83	10.59	267.92	39.32	8.00
3	MC10X6.5	AISC15	29.72	254.00	5.13	3.86	8.81	226.11	31.55	8.55
4	INV_C5x2	Invented	38.00	127.00	5.99	0.99	8.00	99.01	48.01	3.34
5	INV_C20x140	Invented	305.00	508.00	15.01	13.00	19.99	438.00	540.00	1.67
6	INV_C9x23	Invented	140.00	229.01	5.99	5.00	13.00	191.01	242.01	1.64
7	INV_C8x18	Invented	127.00	203.00	5.99	3.99	13.00	165.00	216.00	1.60
8	INV_C14x47.1	Invented	178.00	356.01	10.01	8.00	15.01	305.97	305.97	2.00
9	INV_C20x60	Invented	203.00	508.00	10.01	5.99	19.99	448.01	346.00	2.50
10	INV_C7x13	Invented	114.00	178.00	5.00	0.99	10.01	147.98	197.97	1.56

3.1. Influence of geometric imperfections' period

This study focuses on understanding how the period of the sinusoidal distribution influences cross-sectional behavior. Six distinct local imperfection patterns are analyzed with varying halfwave lengths. To isolate the effect of the number and length of the halfwaves, the amplitude is kept constant across all cases and equal to the 200th of the buckling length per plate ($a_{pp} / 200$: $a_f / 200$ for flanges and $a_w / 200$ for webs). The six types of periods considered herein are summarized in Table 4. Figs. 11 and 12 illustrate histogram plots of the numerical results obtained with both steel grades where the vertical axes correspond to the local buckling reduction factor, χ_L defined by Eq. 4.

$$\chi_L = P_{ult} / P_y \quad (4)$$

Table 4 Characteristics of the various set of sine shapes periods considered

n°	Case	Halfwave length	Amplitude web	Amplitude flange	Half-wave number
1	$HWL = a_{avg} / L = 5a_{avg} / Amp. = a_{pp} / 200$	a_{avg}	$a_w / 200$	$a_f / 200$	5
2	$HWL = a_{avg} / L = 3a_{avg} / Amp. = a_{pp} / 200$	a_{avg}	$a_w / 200$	$a_f / 200$	3
3	$HWL = a_{avg} / L = 2a_{avg} / Amp. = a_{pp} / 200$	a_{avg}	$a_w / 200$	$a_f / 200$	2
4	$HWL = a_f / L = 3a_f / Amp. = a_{pp} / 200$	a_f	$a_w / 200$	$a_f / 200$	3
5	$HWL = a_w / L = 3a_w / Amp. = a_{pp} / 200$	a_w	$a_w / 200$	$a_f / 200$	3
6	$HWL = a_{pp} / L = 3a_{avg} / Amp. = a_{pp} / 200$	a_{pp}	$a_w / 200$	$a_f / 200$	Variable

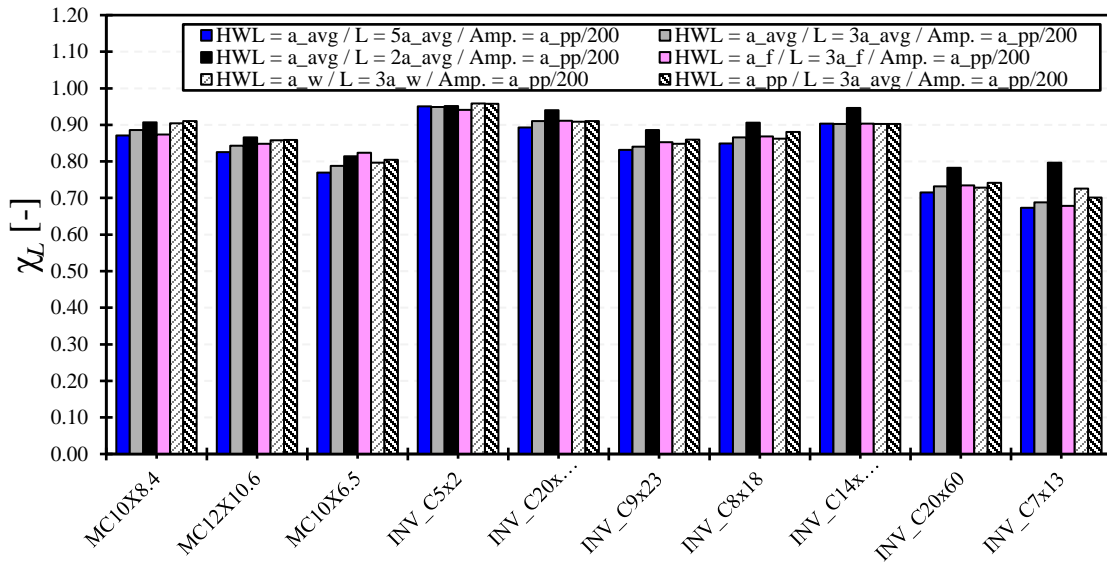


Figure 11: Influence of the period of the sinusoidal imperfection on hot-rolled channel sections under pure compression for $F_y = 260$ MPa

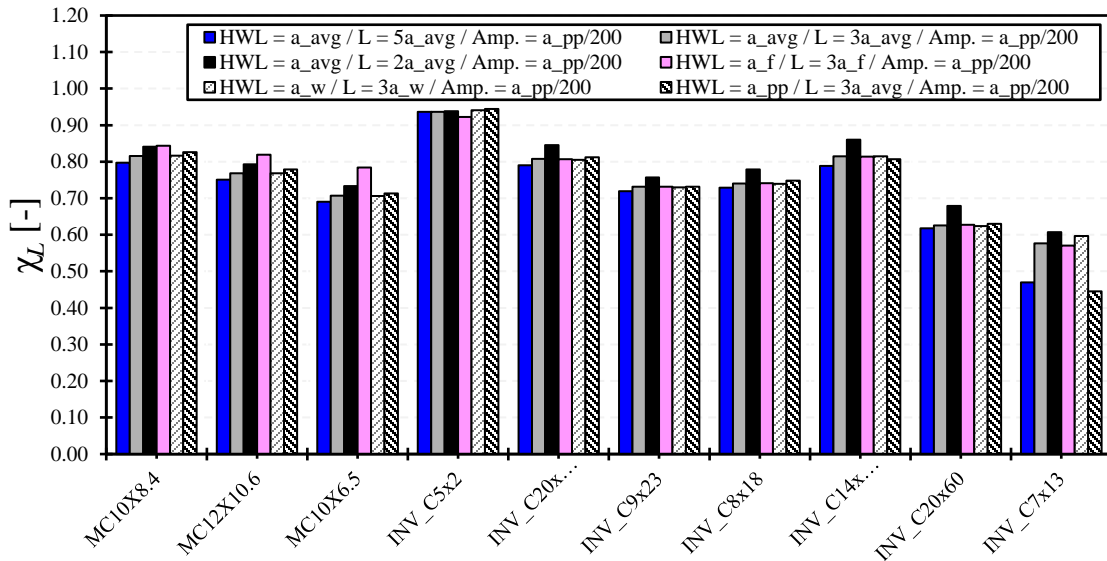


Figure 12: Influence of the period of the sinusoidal imperfection on hot-rolled channel sections under pure compression for $F_y = 400$ MPa

Upon analyzing Figs. 11 and 12, several insights emerge:

- (i). Among cases where the length of the member is equal to 2, 3, and 5 times the average halfwave length, the case with the shortest length ($HWL = a_{avg} / L = 2a_{avg} / Amp. = a_{pp} / 200$) results in higher resistances. This is likely because short members can benefit from support conditions that enhance their overall behavior, thereby increasing resistance. Conversely, the most detrimental effect is achieved with the longest member length, $L = 5a_{avg}$, highlighting a higher likelihood to be subjected to member buckling due to the increased length.
- (ii). When the halfwave length of each plate equals its buckling length ($HWL = a_{pp} / L = 3a_{avg} / Amp. = a_{pp} / 200$), the local imperfection patterns for each cross-section's plate differ. With the member's length not being proportional to the halfwave length of the plates, the imperfection distribution will feature varying numbers of halfwaves in the web and the flanges. As a result, the member will not exhibit full halfwaves over its length.
- (iii). For sections 1 to 3 where the width-to-height ratio, h/b , is significantly higher than the other sections, the case $HWL = a_f / L = 3a_f / Amp. = a_{pp} / 200$ leads to higher resistances than the case $HWL = a_w / L = 3a_w / Amp. = a_{pp} / 200$ with the highest steel grade, $F_y = 400MPa$. As the sensitivity of a plate to local buckling increases with a yield strength, these section's web become slenderer. Moreover, with the buckling length of the flange, a_f , being significantly lower than that of the web, a_w , so that the length of the member is smaller than the height of the web ($L = 3a_f < a_w$), the web is then loaded on its shorter side which increases the energy required to trigger buckling.
- (iv). Overall, the variation in halfwave length has a negligible effect on the compressive resistance because, for cases where the length is three times the halfwave length, no significant discrepancies are observed. The most distinguishable discrepancies were due to the number of halfwaves.

3.2. Influence of geometric imperfections' amplitude

Six cases were investigated to evaluate the influence of the amplitude in a sine-shape local imperfection pattern. For each of the cases defined in Table 5, the halfwave length was kept constant and set to the average of the plates' buckling lengths. This ensured consistency of period and member's length across the different studied cases to focus only on the effect of amplitude. The same cross-sections were examined, and the results are illustrated in Fig. 13 and Fig. 14.

Table 5 Characteristics of the various set of sine shapes amplitudes considered

n°	Case	Halfwave length	Amplitude web	Amplitude flange	Half-wave number
1	$HWL = a_{avg} / L = 3a_{avg} / Amp. = a_{pp} / 100$	a_{avg}	$a_w / 200$	$a_f / 200$	3
2	$HWL = a_{avg} / L = 3a_{avg} / Amp. = a_{pp} / 200$	a_{avg}	$a_w / 100$	$a_f / 100$	3
3	$HWL = a_{avg} / L = 3a_{avg} / Amp. = a_{pp} / 400$	a_{avg}	$a_w / 400$	$a_f / 400$	3
4	$HWL = a_{avg} / L = 3a_{avg} / Amp. = a_{avg} / 200$	a_{avg}	$a_{avg} / 200$	$a_{avg} / 200$	3
5	$HWL = a_{avg} / L = 3a_{avg} / Amp. = a_f / 200$	a_{avg}	$a_f / 200$	$a_f / 200$	3
6	$HWL = a_{avg} / L = 3a_{avg} / Amp. = a_w / 200$	a_{avg}	$a_w / 200$	$a_w / 200$	3

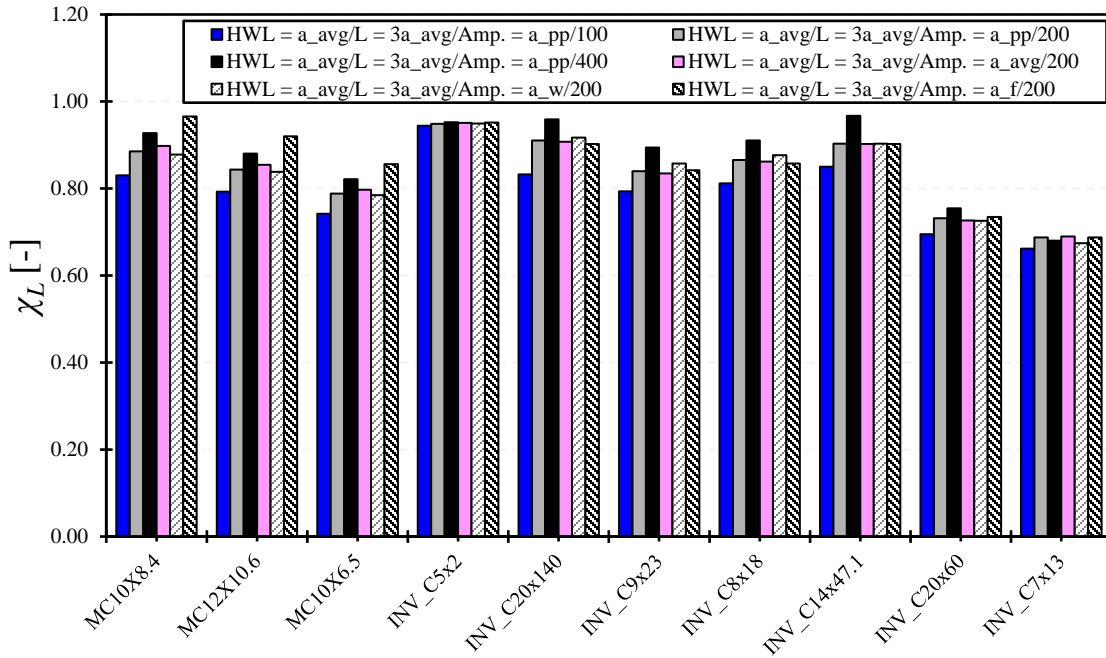


Figure 13: Influence of the amplitude of the sinusoidal imperfection on hot-rolled channel sections under pure compression for $F_y = 260$ MPa

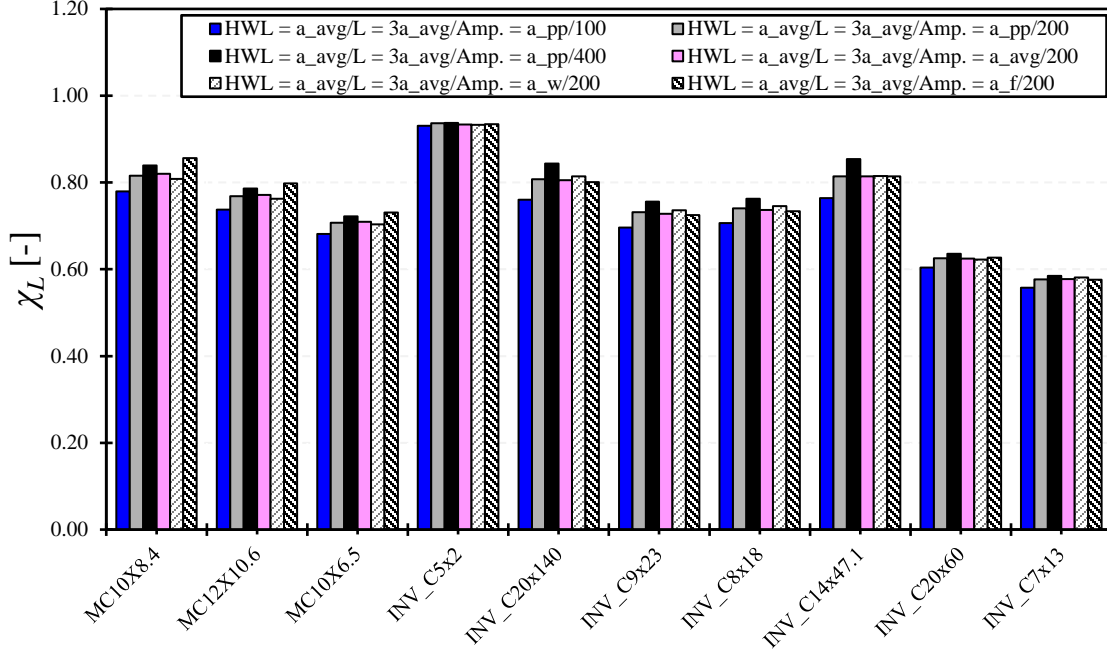


Figure 14: Influence of the amplitude of the sinusoidal imperfection on hot-rolled channel sections under pure compression for $F_y = 400$ MPa

- (i). As expected, among the three first studied cases the highest resistances were observed for $a_{pp} / 400$, while the lowest resistances corresponded to $a_{pp} / 100$ with differences up to 9% for the same cross-section. According to section 2, an amplitude of $a_{pp} / 200$ was proven to be too conservative for members under pure compression with discrepancies up to 12% compared to experimental results. The present study then proves that using an amplitude of $a_{pp} / 400$ rather than $a_{pp} / 200$ will increase the ultimate capacity to up to 7%.
- (ii). Whether the amplitude depends on the individual buckling lengths, a_{pp} or the average of the buckling lengths, a_{avg} , the analyses results in the similar ultimate capacities. Moreover, both cases also lead to similar results with the case where the amplitude depends on the highest buckling length, a_f or a_w .
- (iii). For sections 1 to 4, and 9 where $a_f < a_w$, the case $HWL = a_{avg} / L = 3a_{avg} / Amp. = a_f / 200$ leads to more favorable results than the case $HWL = a_{avg} / L = 3a_{avg} / Amp. = a_w / 200$, and inversely when $a_f > a_w$ for sections 5 to 7, and 10.

3.3. Geometric imperfections through the 1st buckling mode shape as an initial geometric imperfection

The use of buckling modes obtained from a previous linear buckling analysis is one of the most common methods to account for initial geometric imperfections. In this study, only the first buckling mode will be used with an amplification factor corresponding to a proportion of either the average buckling length or the buckling length of either the flanges or the web, with a member

length equal to $3a_{avg}$. The ratios of the ultimate resistances, P_{Eigen} / P_{Sine} , obtained with the eigenmode shapes, and the sine shapes are summarized in Table 6.

Table 6: Comparison of ultimate cross-sectional capacities of hot-rolled channel sections modelled with eigenmode vs sine shapes as local geometric imperfection patterns

	$P_{Eigen} / P_{Sine} [-]$		
	$a_{avg} / 200$	$a_w / 200$	$a_f / 200$
Mean	1.03	1.03	1.02
COV	2.4%	2.7%	2.7%
Min.	1.00	1.00	1.00
Max.	1.09	1.11	1.09
%>1.05	50.0%	40.0%	40.0%
%>1.10	0.0%	10.0%	0.0%

Overall, using the first eigenmode shapes as local geometric imperfection patterns leads to higher cross-sectional resistances than the sine shapes. However, the discrepancies are not so big as the highest mean value of the ratio P_{Eigen} / P_{Sine} is only equal to 1.03 with a COV of .7%. This means that even if the initial shapes differ, the influence of both types of imperfection patterns can be considered equivalent. At the same time, the number of analyses is doubled in the case of eigenmodes as a prior linear buckling analysis is required. Moreover, the comparison of both patterns with respect to an amplitude proportional to a_{pp} could not be made as it is quite difficult to assign amplitudes to the plates individually with this approach.

4. Summary of observations and recommendations for F.E. modeling

The parametric study investigating various sets of local imperfections on the cross-sectional behavior of hot-rolled channel sections has provided valuable insights. Based on the findings and observations, the recommended set of local geometric imperfections is: $HWL = a_{avg} / L = 3a_{avg} / Amp. = a_{pp} / 400$. In this case, the length of the member is set equal to three times the average of the web and flange buckling length, a_{avg} , the sine shape has a halfwave length of a_{avg} and an amplitude equal to $1/400^{\text{th}}$ of each plate's buckling length ($a_f / 400$ for the flange and $a_w / 400$ for the web). While the studies indicate that variations in halfwave lengths have a minimal effect on cross-sectional resistance, the halfwave must consider both web and flange widths. This ensures that all parts of the cross-section have the same number of halfwaves, allowing full halfwaves to develop along the length of the member. This approach maintains consistency and coherence in local imperfections, enhancing the structural integrity of the section.

Although the approach of using the first eigenmode as an imperfection pattern is widely used and as suggested by the results obtained in this study, yields similar results, using sine shapes as geometric imperfection patterns offers better control over the definition of the imperfection parameters, especially the amplitudes of the sine shapes.

5. Conclusions

Geometric and material imperfections significantly influence the resistance of structural members in non-linear analyses. Reliable and consistent results require a generic method for defining these imperfections in finite element models. However, this is a shortcoming observed in current design standards, so this paper aimed to investigate a reliable and consistent local geometric imperfection pattern. Upon validation of the numerical models against experimental data, parametric studies were conducted to assess the influence of different sine shape periods and amplitudes, and the first eigenmode shapes. Results showed that the hot-rolled channel sections under pure compression are more sensitive to the number of halfwaves and amplitudes than the sine shape period. Based on the observations, recommendations on imperfection shapes and amplitudes were provided for safe, convenient, and consistent finite element modeling of hot-rolled channel sections.

References

- American Institute of Steel Construction (2022a) ‘ANSI/AISC 303-22: Code of Standard Practice for Steel Buildings and Bridges’. Chicago, Ill.
- American Institute of Steel Construction (2022b) ‘ANSI/AISC 360-22: Specification for Structural Steel Buildings’. United States of America.
- ASTM International (2023) ‘A6/A6M – 23: Standard Specification for General Requirements for Rolled Structural Steel Bars, Plates, Shapes, and Sheet Piling’. United States of America.
- Beyer, A. (2017) *On the Design of Members with Open Cross Sections Subject to Combined Axial Compression, Bending and Torsion*. PhD thesis. Lorraine University.
- Canadian Standards Association (CSA Group) (2023) ‘G40.20-13/G40.21-13: General requirements for rolled or welded structural quality steel/Structural quality steel’. Canada.
- Canadian Standards Association (CSA Group) (2024) ‘CSA S16:24 - Design and construction of steel structures. Canada.
- Dawson, R.G. and Walker, A.C. (1972) ‘Post-Buckling of Geometrically Imperfect Plates’, *Journal of the Structural Division*, 98(1), pp. 75–94.
- European Committee for Standardization (CEN) (2006) ‘EN 1993-1-5: Eurocode 3 - Design of steel structures - Part 1-5: Plated structural elements.
- Gardner, L. and Nethercot, D.A. (2004) ‘Numerical Modeling of Stainless Steel Structural Components—A Consistent Approach’, *Journal of Structural Engineering*, 130(10), pp. 1586–1601.
- Gérard, L. *et al.* (2019) ‘Recommendations on the geometrical imperfections definition for the resistance of I-sections’, *Journal of Constructional Steel Research*, 162, p. 105716.
- Greiner, R. *et al.* (2009) ‘SEMI-COMP: Plastic member capacity of semi-compact steel sections—a more economic design’, *European Commission, Research Fund for Coal and Steel, Luxembourg: Office for Official Publications of the European Communities* [Preprint].
- Li, L. *et al.* (2022) ‘The Overall Interaction Concept for the design of hot-rolled and welded I-sections under combined loading’, *Thin-Walled Structures*, 172, p. 108623.
- Li, S. (2023) *Behaviour and design of hot-rolled stainless steel channel section members*. PhD thesis. Nanyang Technological University, Singapore.
- Lindner, J. and Glitsch, T. (2004) ‘Vereinfachter Nachweis für I- und U-Träger – beansprucht durch doppelte Biegung und Torsion’, *Stahlbau*, 73(9), pp. 704–715.
- Nseir, J. *et al.* (2016) ‘Influence of imperfections on the local buckling response of hollow structural shapes’, in *Proceedings of the Annual Stability Conference Structural Stability Research Council*. Orlando, Florida.
- Schafer, B.W. and Peköz, T. (1998) ‘Computational modeling of cold-formed steel: characterizing geometric imperfections and residual stresses’, *Journal of Constructional Steel Research*, 47(3), pp. 193–210.
- Snijder, H.H. (Bert) *et al.* (2008) ‘Design rules for lateral torsional buckling of channel sections subject to web loading’, *Stahlbau*, 77(4), pp. 247–256.
- Yun, X. *et al.* (2016) ‘Experimental and numerical investigation into the local imperfection sensitivity of hot-rolled steel I-sections’, p. 18.
- Yun, X. and Gardner, L. (2017) ‘Stress-strain curves for hot-rolled steels’, *Journal of Constructional Steel Research*, 133, pp. 36–46.